EUROPEAN JOURNAL OF PURE AND APPLIED MATHEMATICS
2025, Vol. 18, Issue 2, Article Number 5901
ISSN 1307-5543 – ejpam.com
Published by New York Business Global

Impact of Fractal-Fractional Dynamics on Pneumonia Transmission Modeling

Sayed Saber[1,2], Abdullah A. Alahmari[3,*]

[1] *Mathematics Department, Faculty of Science, Al-Baha University, Saudi Arabia*
[2] *Department of Mathematics and Computer Science, Faculty of Science, Beni-Suef University, Egypt*
[3] *Mathematics Department, Faculty of Science, Umm Al-Qura University, Saudi Arabia*

Abstract. In this study, we develop a fractal-fractional pneumonia transmission model using the Atangana-Baleanu derivative to capture long-memory effects. We analyze the existence and uniqueness of the model's solutions and examine its stability using Hyers-Ulam criteria. Numerical simulations are conducted to explore the influence of different fractional orders on disease dynamics. The results indicate that fractional-order modeling provides a more flexible and accurate framework than classical integer-order models, particularly in representing population heterogeneities and intervention strategies such as vaccination and treatment. This approach enhances our understanding of pneumonia transmission and offers valuable insights for public health decision-making.

2020 Mathematics Subject Classifications: 34A08, 92D30

Key Words and Phrases: Fractal-fractional dynamics, pneumonia transmission, Atangana-Baleanu derivative, long-memory effects

1. Introduction

Pneumonia remains a major public health concern, affecting millions worldwide and leading to severe complications, particularly among young children and the elderly. Traditional epidemiological models, often based on integer-order differential equations, provide valuable insights into disease dynamics but fail to capture complex real-world characteristics such as memory effects, heterogeneity in disease progression, and long-term dependencies in population interactions. These limitations necessitate the exploration of more advanced mathematical frameworks to enhance predictive accuracy and model realism. Pneumonia, a lung disease, affects everyone of varying severity. It is typically diagnosed through physical examinations, a patient history, and diagnostic tests. Pneumonia is characterized by lung inflammation, often caused by microbial or fungal infections, though certain cases arise from inhaling harmful substances. While most pneumococcal toxins are

*Corresponding author.
DOI: https://doi.org/10.29020/nybg.ejpam.v18i2.5901

Email addresses: Sayed011258@science.bsu.edu.eg (S. Saber), aaahmari@uqu.edu.sa (A. A. Alahmari)

harmless, some can cause serious health problems, such as brain damage and hearing loss. Pneumococcal meningitis, the most severe condition, primarily affects children under five years old but also impacts adults. Bacteria causing pneumococcal infections can spread through the bloodstream, and approximately 1% of children under five infected with this disease succumb to it. Additionally, pneumococcal pneumonia is a leading cause of death among the elderly, with a mortality rate of approximately 5%, rising significantly in this population.

Ong'ala et al. [1] developed a mathematical model of bacteremic pneumonia in young children (under five years old) to describe the disease's occurrence. They analyzed transmission rates between carriers and infected individuals using bifurcation theory and equilibrium stability analysis. Mochan et al. [2] proposed a dynamic ordinary differential equation (ODE) model to capture the immunological response to bacterial pneumonia in murine strains. Drusano et al. [3] investigated the role of granulates in preventing bacterial growth and concluded that antibiotics play no role in this specific process. Ndelwa et al. [4] analyzed pneumonia transmission dynamics, incorporating screening and medication, and explored the associated consequences. Kosasih et al. [5] employed a wavelet-based crackling detection technique to model cough sounds, facilitating rapid identification of bacterial pneumonia in young patients.

César et al. [6] presented a mathematical model for pediatric asthma and pneumonia in a large population. Marchello et al. [7] demonstrated that atypical bacterial infections predominantly drive the spread of respiratory illnesses such as coughing, bronchitis, and chronic obstructive pulmonary disease (COPD). Cheng et al. [8] proposed a dynamical mathematical model of influenza A virus secondary pneumonia (IAVSP), providing a quantitative risk assessment framework to improve COPD-related respiratory health. Kosasih et al. [9] discussed diagnostic measures for childhood pneumonia in low-income areas, identifying key contributing factors.

Tilahun et al. [10, 11] introduced a co-infection model for pneumonia and typhoid, examining the interplay of curative and therapeutic strategies. Raj et al. [12] analyzed asthma and pneumonia classification in low-resource settings using mathematical properties of cough sounds. Kizito et al. [13] developed a mathematical model to illustrate how microorganisms inhibit pneumonia spread, examining vaccine formulation and treatment dynamics. Mbabazi et al. [14] presented a nonlinear mathematical model describing the interplay between influenza A virus and pneumonia within the host. Tilahun et al. [15, 16] formulated a pneumonia-meningitis co-infection model using ODEs and highlighted disease eradication strategies. Diah et al. [17] evaluated pneumonia risk using dynamic mathematical models. Mbabazi et al. [18] proposed a Hopf-bifurcation analysis to study pneumococcal pneumonia with temporal delays. Otoo et al. [19] examined the efficacy of bacterial pneumonia transmission models, emphasizing immunization's role in disease prevention. Zephaniah et al. [20] provided graphical representations of dynamic pneumonia models. Ming et al. [21] reported the rise of Coronavirus pneumonia in Wuhan, China, confirmed by clinical testing led by Jung et al. [22]. Wafula et al. [23] developed a deterministic model for pneumonia-HIV co-infection, incorporating anti-pneumonia and ART therapies as optimal controls. Oluwatobi et al. [24] investigated pneumonia transmission

dynamics, fundamental reproduction numbers, and equilibrium points. Sayed Saber et al. [25, 26] proposed a fractional SVCIR model to analyze pneumonia spread. Muhammad Naveed et al. [27] examined a delayed variant of the SCIR model and conducted its mathematical analysis. Many mathematical models have been solved by analytical and numerical methods such as VIM, ADM, etc, [28–31].

Fractional calculus has gained significant attention for its applications in engineering [32], plant epidemiology [33], mathematical biology [34], medicine [35], as well as psychological and life sciences [36]. Several types of fractional derivatives are used in this field, including the Riemann-Liouville, Caputo, Caputo-Fabrizio, and Atangana-Baleanu operators. These have applications in physics [37–46], viscoelasticity [47], electromagnetic wave propagation [48], quantum dynamics [49], Langevin systems [50], Diabetes [51–56]. Fractal-fractional (FF) models describe complex, real-world phenomena effectively. They have been extensively studied in various systems, including excitation-relaxation and natural oscillatory systems [57–61]. FF models provide superior accuracy to traditional integer-order models by capturing long-memory behaviors, heavy-tailed distributions, and short-range autocorrelation dependencies. The Atangana-Baleanu fractal-fractional operator, which integrates fractal geometry into the fractional calculus framework, has been instrumental in analyzing pneumonia dynamics. This operator helps identify infection mechanisms, improve treatment strategies, and gain insights into pneumonia pathogenesis. With Atangana-Baleanu fractal-fractional operators, infectious disease spread, vaccine and drug efficacy, and public health interventions can be studied. In addition, masks are used and contact tracing is done. These operators also enable policymakers to assess intervention impacts and develop long-term mitigation strategies. The paper analyzes a mathematical model for pneumonia using fractal-fractional operators. The novelty of this study lies in extending previous results to fractal-fractional models and demonstrating enhanced accuracy and predictive capabilities.

This study presents a novel fractal-fractional pneumonia transmission model incorporating the Atangana-Baleanu derivative, offering a more accurate representation of disease dynamics compared to traditional integer-order and classical fractional models. The results demonstrate that our approach captures long-memory effects and population heterogeneity more effectively, leading to improved predictions of disease progression and intervention outcomes. The incorporation of Hyers-Ulam stability analysis further strengthens the theoretical foundation of the model, differentiating it from previous research. Numerical simulations confirm that varying fractional orders significantly influence disease behavior, highlighting the flexibility of the proposed framework. Future research could explore the integration of environmental and social factors into the model, as well as the application of alternative numerical methods to enhance computational efficiency. Additionally, extending the model to other infectious diseases could provide further insights into the role of fractional calculus in epidemiological modeling. The paper analyzes a mathematical model for pneumonia using fractal-fractional operators. The novelty of this study lies in extending previous results to fractal-fractional models and demonstrating enhanced accuracy and predictive capabilities. In this study, we develop a fractal-fractional mathematical model to describe pneumonia transmission, incorporating the Atangana-Baleanu

derivative to account for long-memory effects. We analyze the existence and uniqueness of solutions, investigate the stability of equilibrium points using Hyers-Ulam criteria, and conduct numerical simulations to explore the impact of different fractional orders on disease progression. Our results demonstrate that fractal-fractional models provide a more flexible and accurate framework than classical integer-order models, offering valuable insights into disease control strategies, including vaccination and treatment interventions.

The Atangana-Baleanu fractional derivative was chosen over alternative approaches due to its superior ability to model memory effects and non-locality in real-world epidemiological systems. Unlike the classical Caputo and Riemann-Liouville derivatives, which rely on singular kernels, the Atangana-Baleanu derivative employs a non-singular and non-local Mittag-Leffler kernel. This allows for more accurate representation of long-memory effects and biological processes such as immune response delays and heterogeneous transmission patterns. Additionally, the Atangana-Baleanu approach ensures stability and better numerical convergence, making it more suitable for capturing complex disease dynamics, such as pneumonia spread, compared to other fractional derivatives. The improved flexibility and accuracy provided by this operator justify its selection for this study.

To validate the main theorems of this study, a comparison with previous research is necessary. Traditional integer-order models often fail to capture the long-memory effects inherent in infectious disease dynamics. Studies using classical fractional derivatives, such as the Caputo and Riemann-Liouville approaches, provide improvements but still rely on singular kernels, which limit their applicability in modeling realistic transmission scenarios. In contrast, our model, based on the Atangana-Baleanu derivative, enhances accuracy by incorporating a non-singular, non-local kernel, allowing for more realistic disease dynamics. The stability analysis using Hyers-Ulam criteria further differentiates our work by offering a more rigorous mathematical foundation. Numerical comparisons indicate that our model provides a more flexible and robust framework for predicting disease spread, making it a valuable extension of previous epidemiological models.

The remainder of this paper is structured as follows: Section shows the Preliminary Definitions. Section 3 presents the formulation of the fractal-fractional pneumonia model. Section 4 discusses the theoretical analysis of solution existence. Section 5 discusses the theoretical analysis of solution uniqueness. Section 6 discusses the stability analysis of the model. Section 7 provides numerical simulations and interpretations. Section 5 concludes the conclusion and future research directions.

2. Preliminary Definitions

The fractal-fractional framework extends the SCIR model using the Atangana-Baleanu derivative. The fractal-fractional derivative on (a, b) of order $0 < \varrho_2 \leq 1$ is defined as:

Definition 1 ([57]). *The Atangana-Baleanu fractal-fractional derivative is given by:*

$$^{\mathtt{FF-AB}}\mathscr{D}_t^{\varrho_1,\varrho_2}\epsilon(\mathtt{t}) = \frac{\mathtt{B}^*(\varrho_1)}{1-\varrho_1}\frac{d}{dt^{\varrho_2}}\int_0^t \epsilon(s)E_{\varrho_1}\left[-\frac{\varrho_1}{1-\varrho_1}(\mathtt{t}-s)^{\varrho_1}\right]ds,$$

where $\mathtt{B}^*(\varrho_1) = 1-\varrho_1+\frac{\varrho_1}{\Gamma(\varrho_1)}$ *and* $\frac{d\epsilon(s)}{ds^{\varrho_2}} = \lim_{t\to s}\frac{\epsilon(\mathtt{t})-\epsilon(s)}{t^{\varrho_2}-s^{\varrho_2}}$.

The corresponding fractal-fractional integral is:

Definition 2. *The fractal-fractional integral in the Atangana-Baleanu framework is:*

$$\begin{aligned}{}^{\mathtt{FFM}}I_{0,t}^{\varrho_1,\varrho_2}[g(\mathtt{t})] =& \frac{\varrho_1\varrho_2}{\mathtt{B}^*(\varrho_1)\Gamma(\varrho_1)}\int_0^t \epsilon^{\varrho_2-1}g(\epsilon)(\mathtt{t}-\epsilon)^{\varrho_1-1}d\epsilon \\ &+ \frac{\varrho_2(1-\varrho_1)t^{\varrho_2-1}g(\mathtt{t})}{\mathtt{B}^*(\varrho_1)}.\end{aligned}$$

3. Fractal-Fractional Pneumonia Model Extension

The SCIR model, proposed by Kamaledin Abodayeh et al. in [62], is formulated as follows:

$$\begin{aligned}\frac{d\,\mathrm{S}(\mathtt{t})}{dt} &= \Pi - \lambda\,\mathrm{S}(\mathtt{t}) - \mu\,\mathrm{S}(\mathtt{t}) + \eta\,\mathrm{R}(\mathtt{t}),\\ \frac{d\,\mathrm{C}(\mathtt{t})}{dt} &= \lambda\vartheta\,\mathrm{S}(\mathtt{t}) - (\pi+\beta+\mu)\,\mathrm{C}(\mathtt{t}),\\ \frac{d\,\mathrm{I}(\mathtt{t})}{dt} &= \lambda(1-\vartheta)\,\mathrm{S}(\mathtt{t}) + \pi\,\mathrm{C}(\mathtt{t}) - (\mu+\tau+\sigma)\,\mathrm{I}(\mathtt{t}),\\ \frac{d\,\mathrm{R}(\mathtt{t})}{dt} &= \beta\,\mathrm{C}(\mathtt{t}) + \tau\,\mathrm{I}(\mathtt{t}) - (\mu+\eta)\,\mathrm{R}(\mathtt{t}),\end{aligned} \tag{1}$$

where $\lambda = \frac{\delta(\mathrm{I}(\mathtt{t})+\varpi\,\mathrm{C}(\mathtt{t}))}{N}$. The initial conditions are:

$$\mathrm{S}(0) = \mathrm{S}_0 \geq 0, \quad \mathrm{C}(0) = \mathrm{C}_0 \geq 0, \quad \mathrm{I}(0) = \mathrm{I}_0 \geq 0, \quad \mathrm{R}(0) = \mathrm{R}_0 \geq 0.$$

In this model, $\mathrm{S}(\mathtt{t})$ represents the susceptible population at risk of acquiring pneumonia, $\mathrm{C}(\mathtt{t})$ denotes carriers who may transmit the disease, $\mathrm{I}(\mathtt{t})$ represents infected individuals, and $\mathrm{R}(\mathtt{t})$ denotes recovered individuals. Key parameters are defined as follows: - μ: natural mortality rate,
- Π: recruitment rate to the susceptible population,
- π: recruitment rate into the carrier population,
- ϑ: proportion of susceptibles joining the carrier population,
- σ: disease-induced mortality rate,
- β: recovery rate of carriers,
- τ: recovery rate of infected individuals,
- η: rate of treated individuals becoming susceptible again,
- ϖ: rate of treated individuals becoming vaccinated,
-The transmission coefficient λ represents the infection force, and p is the probability that contact results in infection.

Applying the Atangana-Baleanu operator to the SCIR model yields:

$$\begin{aligned}{}^{\mathtt{FF-AB}}\mathscr{D}_t^{\varrho_1,\varrho_2}\,\mathrm{S}(\mathtt{t}) &= \Pi - \lambda\,\mathrm{S}(\mathtt{t}) - \mu\,\mathrm{S}(\mathtt{t}) + \eta\,\mathrm{R}(\mathtt{t}),\\ {}^{\mathtt{FF-AB}}\mathscr{D}_t^{\varrho_1,\varrho_2}\,\mathrm{C}(\mathtt{t}) &= \lambda\vartheta\,\mathrm{S}(\mathtt{t}) - (\pi+\beta+\mu)\,\mathrm{C}(\mathtt{t}),\\ {}^{\mathtt{FF-AB}}\mathscr{D}_t^{\varrho_1,\varrho_2}\,\mathrm{I}(\mathtt{t}) &= \lambda(1-\vartheta)\,\mathrm{S}(\mathtt{t}) + \pi\,\mathrm{C}(\mathtt{t}) - (\mu+\tau+\sigma)\,\mathrm{I}(\mathtt{t}),\\ {}^{\mathtt{FF-AB}}\mathscr{D}_t^{\varrho_1,\varrho_2}\,\mathrm{R}(\mathtt{t}) &= \beta\,\mathrm{C}(\mathtt{t}) + \tau\,\mathrm{I}(\mathtt{t}) - (\mu+\eta)\,\mathrm{R}(\mathtt{t}).\end{aligned} \tag{2}$$

The system can be expressed in vector form as:

$$^{\mathtt{FF-AB}}\mathscr{D}_{0,\mathtt{t}}^{\varrho_1,\varrho_2}\Psi(\mathtt{t}) = \varrho_2 \mathtt{t}^{\varrho_2-1} W(\mathtt{t},\Psi(\mathtt{t})) = \Xi(\mathtt{t},\Psi(\mathtt{t})),$$

where $\Psi(\mathtt{t}) = (\mathrm{S}(\mathtt{t}), \mathrm{C}(\mathtt{t}), \mathrm{I}(\mathtt{t}), \mathrm{R}(\mathtt{t}))$, and $\Psi(0) = (\mathrm{S}(0), \mathrm{C}(0), \mathrm{I}(0), \mathrm{R}(0))$, and $W(\mathtt{t},\Psi(\mathtt{t})) = (W_1(\mathtt{t},\Psi(\mathtt{t})), W_2(\mathtt{t},\Psi(\mathtt{t})), W_3(\mathtt{t},\Psi(\mathtt{t})), W_4(\mathtt{t},\Psi(\mathtt{t})))$, with

$$\begin{aligned}
W_1(\mathtt{t},S) &= \Pi - \lambda\,\mathrm{S} - \mu\,\mathrm{S} + \eta\,\mathrm{R},\\
W_2(\mathtt{t},C) &= \lambda\vartheta\,\mathrm{S} - (\pi+\beta+\mu)\,\mathrm{C},\\
W_3(\mathtt{t},\mathrm{I}) &= \lambda(1-\vartheta)\,\mathrm{S} + \pi\,\mathrm{C} - (\mu+\tau+\sigma)\,\mathrm{I},\\
W_4(\mathtt{t},R) &= \beta\,\mathrm{C} + \tau\,\mathrm{I} - (\mu+\eta)\,\mathrm{R}\,.
\end{aligned} \tag{3}$$

4. Existence of the model solutions

By $\mathbb{R}_+$, we refer to the set of all positive real numbers, $\Omega = \{(\mathrm{S},\mathrm{C},\mathrm{I},\mathrm{R}) \in \mathbb{R}_+^4 : \mathrm{S} \geq 0,\ \mathrm{C} \geq 0,\ \mathrm{I} \geq 0,\ \mathrm{R} \geq 0,\ \max(|\,\mathrm{S}\,|, |\,\mathrm{C}\,|, |\,\mathrm{I}\,|, |R|) \leq N\}$. When the fixed point theory is applied and the fractal-fractional integral operator is utilized, the constructed model (2) can be converted into an integral equation.

$$\begin{aligned}
\mathrm{S}(\mathtt{t}) - \mathrm{S}(0) &= \frac{\varrho_2(1-\varrho_1)t^{\varrho_2-1}}{\mathtt{B}^*(\varrho_1)}(\Pi - \lambda\,\mathrm{S} - \mu\,\mathrm{S} + \eta\,\mathrm{R})\\
&\quad + \frac{\varrho_1\varrho_2}{\mathtt{B}^*(\varrho_1)\Gamma(\varrho_1)}\int_0^t \epsilon^{\varrho_2-1}(\mathtt{t}-\epsilon)^{\varrho_1-1}(\Pi - \lambda\,\mathrm{S} - \mu\,\mathrm{S} + \eta\,\mathrm{R})d\epsilon,\\
\mathrm{C}(\mathtt{t}) - \mathrm{C}(0) &= \frac{\varrho_2(1-\varrho_1)t^{\varrho_2-1}}{\mathtt{B}^*(\varrho_1)}(\lambda\vartheta\,\mathrm{S} - (\pi+\beta+\mu)\,\mathrm{C})\\
&\quad + \frac{\varrho_1\varrho_2}{\mathtt{B}^*(\varrho_1)\Gamma(\varrho_1)}\int_0^t \epsilon^{\varrho_2-1}(\mathtt{t}-\epsilon)^{\varrho_1-1}(\lambda\vartheta\,\mathrm{S} - (\pi+\beta+\mu)\,\mathrm{C})d\epsilon,\\
\mathrm{I}(\mathtt{t}) - \mathrm{I}(0) &= \frac{\varrho_2(1-\varrho_1)t^{\varrho_2-1}}{\mathtt{B}^*(\varrho_1)}(\lambda(1-\vartheta)\,\mathrm{S} + \pi\,\mathrm{C} - (\mu+\tau+\sigma)\,\mathrm{I})\\
&\quad + \frac{\varrho_1\varrho_2}{\mathtt{B}^*(\varrho_1)\Gamma(\varrho_1)}\int_0^t \epsilon^{\varrho_2-1}(\mathtt{t}-\epsilon)^{\varrho_1-1}(\lambda(1-\vartheta)\,\mathrm{S} + \pi\,\mathrm{C} - (\mu+\tau+\sigma)\,\mathrm{I})d\epsilon,\\
\mathrm{R}(\mathtt{t}) - \mathrm{R}(0) &= \frac{\varrho_2(1-\varrho_1)t^{\varrho_2-1}}{\mathtt{B}^*(\varrho_1)}(\beta\,\mathrm{C} + \tau\,\mathrm{I} - (\mu+\eta)\,\mathrm{R})\\
&\quad + \frac{\varrho_1\varrho_2}{\mathtt{B}^*(\varrho_1)\Gamma(\varrho_1)}\int_0^t \epsilon^{\varrho_2-1}(\mathtt{t}-\epsilon)^{\varrho_1-1}(\beta\,\mathrm{C} + \tau\,\mathrm{I} - (\mu+\eta)\,\mathrm{R})d\epsilon.
\end{aligned}$$

To be able to derive our results, we need to take into consideration the following assumptions:

(Q^*): Let assume that $\mathrm{S}(\mathtt{t}), \mathrm{C}(\mathtt{t}), \mathrm{I}(\mathtt{t})$ and $\mathrm{R}(\mathtt{t})$ are bounded satisfies $\|\,\mathrm{S}(\mathtt{t})\| \leq \xi_1$, $\|\,\mathrm{C}(\mathtt{t})\| \leq \xi_2$, $\|\,\mathrm{I}(\mathtt{t})\| \leq \xi_1$, $\|\,\mathrm{R}(\mathtt{t})\| \leq \xi_2$.

Lemma 1. *The kernels W_i fulfill Lipschitz condition under the assumption (Q^*) and $\varphi_i < 1$, for $i \in \mathbb{N}_1^4$.*

Proof.

$$\begin{aligned}\|W_1(\mathtt{t},S)-W_1(\mathtt{t},\mathrm{S}_1)\| &= \|(\Pi-\lambda\,\mathrm{S}-\mu\,\mathrm{S}+\eta\,\mathrm{R})-(\Pi-\lambda\,\mathrm{S}^{**}-\mu\mathtt{S}^{*}+\eta\,\mathrm{R})\|\\ &\leq (|\lambda|+\mu)\|(S-\mathrm{S}_1)\|\\ &\leq \varphi_1\|S-\mathrm{S}_1\|,\end{aligned}$$

where $\varphi_1=\delta+\varpi+\mu$.

$$\begin{aligned}.\|W_2(\mathtt{t},C)-W_2(\mathtt{t},\mathrm{C}_1))\| &= \|(\lambda\vartheta\,\mathrm{S}-(\pi+\beta+\mu)\,\mathrm{C})-(\lambda\vartheta\,\mathrm{S}-(\pi+\beta+\mu)\,\mathrm{C}^{**})\|\\ &\leq \varphi_2\|C-\mathrm{C}_1\|,\end{aligned}$$

where $\varphi_2=\mu+\beta+\pi$.

$$\begin{aligned}\|W_3(\mathtt{t},\mathrm{I})-W_3(\mathtt{t},\mathrm{I}_1)\| &= \|\lambda(1-\vartheta)\,\mathrm{S}+\pi\,\mathrm{C}-(\mu+\tau+\sigma)\,\mathrm{I})\\ &\quad-(\lambda(1-\vartheta)\,\mathrm{S}+\pi\,\mathrm{C}-(\mu+\tau+\sigma)\,\mathrm{I}_1)\|\\ &\leq \varphi_3\|\,\mathrm{I}-\mathrm{I}_1\|,\end{aligned}$$

where $\varphi_3=\tau+\mu+\sigma$.

$$\begin{aligned}.\|W_4(\mathtt{t},R)-W_4(\mathtt{t},\mathrm{R}_1))\| &= \|(\beta\,\mathrm{C}+\tau\,\mathrm{I}-(\mu+\eta)\,\mathrm{R})-(\beta\,\mathrm{C}+\tau\,\mathrm{I}-(\mu+\eta)\,\mathrm{R}^{**})\|\\ &\leq \varphi_4\|(\mathrm{R}-\mathrm{R}_1)\|,\end{aligned}$$

where $\varphi_4=\mu+\eta$. Thus, we have that W_i for $i=1,2,3,4$, satisfy the Lipschitz property and the result is accomplished.

Considering W_1, W_2, W_3, and W_4 in (3) with initial conditions $S(0)=\mathrm{S}_0$, $C(0)=C_0$, $I(0)=I_0$, $R(0)=R_0$, using fractal- fractional,

$$\mathrm{S}(\mathtt{t})-\mathrm{S}(0)=\frac{\varrho_2(1-\varrho_1)t^{\varrho_2-1}}{\mathtt{B}^{*}(\varrho_1)}W_1(\mathtt{t},\mathrm{S}(\mathtt{t}))+\frac{\varrho_1\varrho_2}{\mathtt{B}^{*}(\varrho_1)\Gamma(\varrho_1)}\int_0^t\epsilon^{\varrho_2-1}(\mathtt{t}-\epsilon)^{\varrho_1-1}W_1(\epsilon,S(\epsilon))d\epsilon,$$

$$\mathrm{C}(\mathtt{t})-\mathrm{C}(0)=\frac{\varrho_2(1-\varrho_1)t^{\varrho_2-1}}{\mathtt{B}^{*}(\varrho_1)}W_2(\mathtt{t},\mathrm{C}(\mathtt{t}))+\frac{\varrho_1\varrho_2}{\mathtt{B}^{*}(\varrho_1)\Gamma(\varrho_1)}\int_0^t\epsilon^{\varrho_2-1}(\mathtt{t}-\epsilon)^{\varrho_1-1}W_2(\epsilon,C(\epsilon))d\epsilon,$$

$$\mathrm{I}(\mathtt{t})-\mathrm{I}(0)=\frac{\varrho_2(1-\varrho_1)t^{\varrho_2-1}}{\mathtt{B}^{*}(\varrho_1)}W_3(\mathtt{t},\mathrm{I}(\mathtt{t}))+\frac{\varrho_1\varrho_2}{\mathtt{B}^{*}(\varrho_1)\Gamma(\varrho_1)}\int_0^t\epsilon^{\varrho_2-1}(\mathtt{t}-\epsilon)^{\varrho_1-1}W_3(\epsilon,I(\epsilon))d\epsilon,$$

$$\mathrm{R}(\mathtt{t})-\mathrm{R}(0)=\frac{\varrho_2(1-\varrho_1)t^{\varrho_2-1}}{\mathtt{B}^{*}(\varrho_1)}W_4(\mathtt{t},\mathrm{R}(\mathtt{t}))+\frac{\varrho_1\varrho_2}{\mathtt{B}^{*}(\varrho_1)\Gamma(\varrho_1)}\int_0^t\epsilon^{\varrho_2-1}(\mathtt{t}-\epsilon)^{\varrho_1-1}W_4(\epsilon,R(\epsilon))d\epsilon.$$

The iterative scheme of model (2) should be defined as follows:

$$\begin{aligned}
\mathrm{S}_n(\mathtt{t}) - \mathrm{S}(0) &= \frac{\varrho_2(1-\varrho_1)t^{\varrho_2-1}}{\mathtt{B}^*(\varrho_1)} W_1(\mathtt{t}, \mathrm{S}_{n-1}(\mathtt{t})) \\
&\quad + \frac{\varrho_1\varrho_2}{\mathtt{B}^*(\varrho_1)\Gamma(\varrho_1)} \int_0^t \epsilon^{\varrho_2-1}(\mathtt{t}-\epsilon)^{\varrho_1-1} W_1(\epsilon, \mathrm{S}_{n-1}(\epsilon))d\epsilon, \\
\mathrm{C}_n(\mathtt{t}) - \mathrm{C}(0) &= \frac{\varrho_2(1-\varrho_1)t_2\varrho_2 - 1}{\mathtt{B}^*(\varrho_1)} W_2(\mathtt{t}, C_{n-1}(\mathtt{t})) \\
&\quad + \frac{\varrho_1\varrho_2}{\mathtt{B}^*(\varrho_1)\Gamma(\varrho_1)} \int_0^t \epsilon^{\varrho_2-1}(\mathtt{t}-\epsilon)^{\varrho_1-1} W_2(\epsilon, C_{n-1}(\epsilon))d\epsilon, \\
\mathrm{I}_n(\mathtt{t}) - \mathrm{I}(0) &= \frac{\varrho_2(1-\varrho_1)t_2\varrho_2 - 1}{\mathtt{B}^*(\varrho_1)} W_3(\mathtt{t}, I_{n-1}(\mathtt{t})) \\
&\quad + \frac{\varrho_1\varrho_2}{\mathtt{B}^*(\varrho_1)\Gamma(\varrho_1)} \int_0^t \epsilon^{\varrho_2-1}(\mathtt{t}-\epsilon)^{\varrho_1-1} W_3(\epsilon, I_{n-1}(\epsilon))d\epsilon, \\
\mathrm{R}_n(\mathtt{t}) - \mathrm{R}(0) &= \frac{\varrho_2(1-\varrho_1)t_2\varrho_2 - 1}{\mathtt{B}^*(\varrho_1)} W_4(\mathtt{t}, R_{n-1}(\mathtt{t})) \\
&\quad + \frac{\varrho_1\varrho_2}{\mathtt{B}^*(\varrho_1)\Gamma(\varrho_1)} \int_0^t \epsilon^{\varrho_2-1}(\mathtt{t}-\epsilon)^{\varrho_1-1} W_4(\epsilon, R_{n-1}(\epsilon))d\epsilon.
\end{aligned}$$

We now examine the differences in the following manner:

$$\Delta\, \mathrm{S}_{n+1}(\mathtt{t}) = \mathrm{S}_{n+1}(\mathtt{t}) - \mathrm{S}_n(\mathtt{t}),$$

with

$$\begin{aligned}
\Delta\, \mathrm{S}_{n+1}(\mathtt{t}) &= \frac{\varrho_2(1-\varrho_1)t_2 - 1}{\mathtt{B}^*(\varrho_1)} W_1(\mathtt{t}, \mathrm{S}_n(\mathtt{t})) \\
&\quad + \frac{\varrho_1\varrho_2}{\mathtt{B}^*(\varrho_1)\Gamma(\varrho_1)} \int_0^t \epsilon^{\varrho_2-1}(\mathtt{t}-\epsilon)^{\varrho_1-1} W_1(\epsilon, \mathrm{S}_n(\epsilon))d\epsilon \\
&\quad - \Big(\frac{\varrho_2(1-\varrho_1)t_2 - 1}{\mathtt{B}^*(\varrho_1)} W_1(\mathtt{t}, \mathrm{S}_{n-1}(\mathtt{t})) \\
&\quad + \frac{\varrho_1\varrho_2}{\mathtt{B}^*(\varrho_1)\Gamma(\varrho_1)} \int_0^t \epsilon^{\varrho_2-1}(\mathtt{t}-\epsilon)^{\varrho_1-1} W_1(\epsilon, \mathrm{S}_{n-1}(\epsilon))d\epsilon\Big) \\
&= \frac{\varrho_2(1-\varrho_1)t_2 - 1}{\mathtt{B}^*(\varrho_1)} (W_1(\mathtt{t}, \mathrm{S}_n(\mathtt{t})) - W_1(\mathtt{t}, \mathrm{S}_{n-1}(\mathtt{t}))) \\
&\quad + \frac{\varrho_1\varrho_2}{\mathtt{B}^*(\varrho_1)\Gamma(\varrho_1)} \int_0^t \epsilon^{\varrho_2-1}(\mathtt{t}-\epsilon)^{\varrho_1-1} (W_1(\epsilon, \mathrm{S}_n(\epsilon)) - W_1(\epsilon, \mathrm{S}_{n-1}(\epsilon)))d\epsilon,
\end{aligned}$$

and

$$\Delta C_{n+1}(\mathtt{t}) = C_{n+1}(\mathtt{t}) - C_n(\mathtt{t}),$$

with

$$\begin{aligned}\Delta C_{n+1}(\mathtt{t}) &= \frac{\varrho_2(1-\varrho_1)t^{\varrho_2-1}}{\mathtt{B}^*(\varrho_1)}W_2(\mathtt{t},C_n(\mathtt{t}))\\ &+\frac{\varrho_1\varrho_2}{\mathtt{B}^*(\varrho_1)\Gamma(\varrho_1)}\int_0^t \epsilon^{\varrho_2-1}(\mathtt{t}-\epsilon)^{\varrho_1-1}W_2(\epsilon,C_n(\epsilon))d\epsilon\\ &-(\frac{\varrho_2(1-\varrho_1)t^{\varrho_2-1}}{\mathtt{B}^*(\varrho_1)}W_2(\mathtt{t},C_{n-1}(\mathtt{t}))\\ &+\frac{\varrho_1\varrho_2}{\mathtt{B}^*(\varrho_1)\Gamma(\varrho_1)}\int_0^t \epsilon^{\varrho_2-1}(\mathtt{t}-\epsilon)^{\varrho_1-1}W_2(\epsilon,C_{n-1}(\epsilon))d\epsilon)\\ &=\frac{\varrho_2(1-\varrho_1)t^{\varrho_2-1}}{\mathtt{B}^*(\varrho_1)}(W_2(\mathtt{t},I_n(\mathtt{t}))-W_2(\mathtt{t},I_{n-1}(\mathtt{t})))\\ &+\frac{\varrho_1\varrho_2}{\mathtt{B}^*(\varrho_1)\Gamma(\varrho_1)}\int_0^t \epsilon^{\varrho_2-1}(\mathtt{t}-\epsilon)^{\varrho_1-1}(W_2(\epsilon,C_n(\epsilon))-W_2(\epsilon,C_{n-1}(\epsilon)))d\epsilon,\end{aligned}$$

and

$$\Delta I_{n+1}(\mathtt{t}) = I_{n+1}(\mathtt{t}) - I_n(\mathtt{t}),$$

with

$$\begin{aligned}\Delta I_{n+1}(\mathtt{t}) &= \frac{\varrho_2(1-\varrho_1)t^{\varrho_2-1}}{\mathtt{B}^*(\varrho_1)}W_3(\mathtt{t},I_n(\mathtt{t}))\\ &+\frac{\varrho_1\varrho_2}{\mathtt{B}^*(\varrho_1)\Gamma(\varrho_1)}\int_0^t \epsilon^{\varrho_2-1}(\mathtt{t}-\epsilon)^{\varrho_1-1}W_3(\epsilon,I_n(\epsilon))d\epsilon\\ &-(\frac{\varrho_2(1-\varrho_1)t^{\varrho_2-1}}{\mathtt{B}^*(\varrho_1)}W_3(\mathtt{t},I_{n-1}(\mathtt{t}))\\ &+\frac{\varrho_1\varrho_2}{\mathtt{B}^*(\varrho_1)\Gamma(\varrho_1)}\int_0^t \epsilon^{\varrho_2-1}(\mathtt{t}-\epsilon)^{\varrho_1-1}W_3(\epsilon,I_{n-1}(\epsilon))d\epsilon)\\ &=\frac{\varrho_2(1-\varrho_1)t^{\varrho_2-1}}{\mathtt{B}^*(\varrho_1)}(W_3(\mathtt{t},I_n(\mathtt{t}))-W_3(\mathtt{t},I_{n-1}(\mathtt{t})))\\ &+\frac{\varrho_1\varrho_2}{\mathtt{B}^*(\varrho_1)\Gamma(\varrho_1)}\int_0^t \epsilon^{\varrho_2-1}(\mathtt{t}-\epsilon)^{\varrho_1-1}(W_3(\epsilon,I_n(\epsilon))-W_3(\epsilon,I_{n-1}(\epsilon)))d\epsilon,\end{aligned}$$

and

$$\Delta R_{n+1}(\mathtt{t}) = R_{n+1}(\mathtt{t}) - R_n(\mathtt{t}),$$

with

$$\begin{aligned}\Delta R_{n+1}(\mathtt{t}) &= \frac{\varrho_2(1-\varrho_1)t^{\varrho_2-1}}{\mathtt{B}^*(\varrho_1)}W_4(\mathtt{t},R_n(\mathtt{t}))\\ &\quad+\frac{\varrho_1\varrho_2}{\mathtt{B}^*(\varrho_1)\Gamma(\varrho_1)}\int_0^t\epsilon^{\varrho_2-1}(\mathtt{t}-\epsilon)^{\varrho_1-1}W_4(\epsilon,R_n(\epsilon))d\epsilon\\ &\quad-(\frac{\varrho_2(1-\varrho_1)t^{\varrho_2-1}}{\mathtt{B}^*(\varrho_1)}W_4(\mathtt{t},R_{n-1}(\mathtt{t}))\\ &\quad+\frac{\varrho_1\varrho_2}{\mathtt{B}^*(\varrho_1)\Gamma(\varrho_1)}\int_0^t\epsilon^{\varrho_2-1}(\mathtt{t}-\epsilon)^{\varrho_1-1}W_4(\epsilon,R_{n-1}(\epsilon))d\epsilon)\\ &=\frac{\varrho_2(1-\varrho_1)t^{\varrho_2-1}}{\mathtt{B}^*(\varrho_1)}(W_4(\mathtt{t},R_n(\mathtt{t}))-W_4(\mathtt{t},I_{n-1}(\mathtt{t})))\\ &\quad+\frac{\varrho_1\varrho_2}{\mathtt{B}^*(\varrho_1)\Gamma(\varrho_1)}\int_0^t\epsilon^{\varrho_2-1}(\mathtt{t}-\epsilon)^{\varrho_1-1}(W_4(\epsilon,R_n(\epsilon))-W_4(\epsilon,R_{n-1}(\epsilon)))d\epsilon.\end{aligned}$$

Using the norms, we are able to get the following result:

$$\begin{aligned}\|\Delta\,\mathrm{S}_{n+1}(\mathtt{t})\| &= \|\frac{\varrho_2(1-\varrho_1)t^{\varrho_2-1}}{\mathtt{B}^*(\varrho_1)}(W_1(\mathtt{t},\mathrm{S}_n(\mathtt{t}))-W_1(\mathtt{t},\mathrm{S}_{n-1}(\mathtt{t})))\\ &\quad+\frac{\varrho_1\varrho_2}{\mathtt{B}^*(\varrho_1)\Gamma(\varrho_1)}\int_0^t\epsilon^{\varrho_2-1}(\mathtt{t}-\epsilon)^{\varrho_1-1}(W_1(\epsilon,\mathrm{S}_n(\epsilon))-W_1(\epsilon,\mathrm{S}_{n-1}(\epsilon)))d\epsilon\|,\\ \|\Delta C_{n+1}(\mathtt{t})\| &= \|\frac{\varrho_2(1-\varrho_1)t^{\varrho_2-1}}{\mathtt{B}^*(\varrho_1)}(W_2(\mathtt{t},C_n(\mathtt{t}))-W_2(\mathtt{t},C_{n-1}(\mathtt{t})))\\ &\quad+\frac{\varrho_1\varrho_2}{\mathtt{B}^*(\varrho_1)\Gamma(\varrho_1)}\int_0^t\epsilon^{\varrho_2-1}(\mathtt{t}-\epsilon)^{\varrho_1-1}(W_2(\epsilon,C_n(\epsilon))-W_2(\epsilon,C_{n-1}(\epsilon)))d\epsilon\|,\\ \|\Delta I_{n+1}(\mathtt{t})\| &= \|\frac{\varrho_2(1-\varrho_1)t^{2-1}}{\mathtt{B}^*(\varrho_1)}(W_3(\mathtt{t},I_n(\mathtt{t}))-W_3(\mathtt{t},I_{n-1}(\mathtt{t})))\\ &\quad+\frac{\varrho_1\varrho_2}{\mathtt{B}^*(\varrho_1)\Gamma(\varrho_1)}\int_0^t\epsilon^{\varrho_2-1}(\mathtt{t}-\epsilon)^{\varrho_1-1}(W_3(\epsilon,I_n(\epsilon))-W_3(\epsilon,I_{n-1}(\epsilon)))d\epsilon\|,\\ \|\Delta R_{n+1}(\mathtt{t})\| &= \|\frac{\varrho_2(1-\varrho_1)t^{\varrho_2-1}}{\mathtt{B}^*(\varrho_1)}(W_4(\mathtt{t},R_n(\mathtt{t}))-W_4(\mathtt{t},\mathrm{S}_{n-1}(\mathtt{t})))\\ &\quad+\frac{\varrho_1\varrho_2}{\mathtt{B}^*(\varrho_1)\Gamma(\varrho_1)}\int_0^t\epsilon^{\varrho_2-1}(\mathtt{t}-\epsilon)^{\varrho_1-1}(W_4(\epsilon,R_n(\epsilon))-W_4(\epsilon,R_{n-1}(\epsilon)))d\epsilon\|.\end{aligned}$$

Lemma 2. *Based on the assumption (Q^*), model (2) admits a solution whenever*

$$\kappa=\max\{\varphi_1,\varphi_2,\varphi_3,\varphi_4\}<1,$$

for φ_i as defined in the proof of Lemma 1, for i = 1, 2, 3, 4.

Proof. Define four functions, $Z_{1n}(\mathtt{t})$, $Z_{2n}(\mathtt{t})$, $Z_{3n}(\mathtt{t})$ and $Z_{4n}(\mathtt{t})$, as

$$\begin{aligned} Z_{1n}(\mathtt{t}) &= \mathrm{S}_{n+1}(\mathtt{t}) - \mathrm{S}(\mathtt{t}), \\ Z_{2n}(\mathtt{t}) &= C_{n+1}(\mathtt{t}) - \mathrm{C}(\mathtt{t}), \\ Z_{3n}(\mathtt{t}) &= I_{n+1}(\mathtt{t}) - \mathrm{I}(\mathtt{t}), \\ Z_{4n}(\mathtt{t}) &= R_{n+1}(\mathtt{t}) - \mathrm{R}(\mathtt{t}). \end{aligned}$$

As a result

$$\begin{aligned} \|Z_{1n}(\mathtt{t})\| &= \|\frac{\varrho_2(1-\varrho_1)t^{\varrho_2-1}}{\mathtt{B}^*(\varrho_1)}(W_1(\mathtt{t},\mathrm{S}_n(\mathtt{t})) - W_1(\mathtt{t},\mathrm{S}(\mathtt{t}))) \\ &+ \frac{\varrho_1\varrho_2}{\mathtt{B}^*(\varrho_1)\Gamma(\varrho_1)}\int_0^t \epsilon^{\varrho_2-1}(\mathtt{t}-\epsilon)^{\varrho_1-1}(W_1(\epsilon,\mathrm{S}_n(\epsilon)) - W_1(\epsilon,S(\epsilon)))d\epsilon\| \\ &\leq \frac{\varrho_2(1-\varrho_1)t^2-1}{\mathtt{B}^*(\varrho_1)}\|W_1(\mathtt{t},\mathrm{S}_n(\mathtt{t})) - W_1(\mathtt{t},\mathrm{S}(\mathtt{t}))\| \\ &+ \frac{\varrho_1\varrho_2}{\mathtt{B}^*(\varrho_1)\Gamma(\varrho_1)}\int_0^t \epsilon^{\varrho_2-1}(\mathtt{t}-\epsilon)^{\varrho_1-1}\|W_1(\epsilon,\mathrm{S}_n(\epsilon)) - W_1(\epsilon,S(\epsilon))\|d\epsilon \\ &\leq \frac{\varrho_2(1-\varrho_1)t^{\varrho_2-1}}{\mathtt{B}^*(\varrho_1)}\varphi_1\|\,\mathrm{S}_n - \mathrm{S}\,\| \\ &+ \frac{\varrho_1}{\mathtt{B}^*(\varrho_1)\Gamma(\varrho_1)}\int_0^t \epsilon^{\varrho_2-1}(\mathtt{t}-\epsilon)^{\varrho_1-1}\varphi_1\|\,\mathrm{S}_n - \mathrm{S}\,\|d\epsilon \\ &\leq (\frac{\varrho_2(1-\varrho_1)}{\mathtt{B}^*(\varrho_1)} + \frac{\varrho_1\varrho_2\Gamma(\varrho_2)}{\mathtt{B}^*(\varrho_1)\Gamma(\varrho_1+\varrho_2)})\varphi_1\|\,\mathrm{S}_n - \mathrm{S}\,\| \\ &\leq (\frac{\varrho_2(1-\varrho_1)}{\mathtt{B}^*(\varrho_1)} + \frac{\varrho_1\varrho_2\Gamma(\varrho_2)}{\mathtt{B}^*(\varrho_1)\Gamma(\varrho_1+\varrho_2)})^n\varphi_1^n\|\,\mathrm{S}_1 - \mathrm{S}\,\|, \end{aligned}$$

in which for $\varphi_1 < 1$ and as $n \to \infty$, we have $\mathrm{S}_n \to S$. Similarly

$$\begin{aligned} \|Z_{2_n}(t)\| &\leq \left[\frac{\varrho_1\varrho_2\Gamma(\varrho_2)}{\mathtt{B}^*(\varrho_1)\Gamma(\varrho_1+\varrho_2)} + \frac{\varrho_2(1-\varrho_1)}{\mathtt{B}^*(\varrho_1)}\right]^n \varphi_2^n\,\|\mathrm{C}_1 - \mathrm{C}\|\,, \\ \|Z_{3_n}(t)\| &\leq \left[\frac{\varrho_1\varrho_2\Gamma(\varrho_2)}{\mathtt{B}^*(\varrho_1)\Gamma(\varrho_1+\varrho_2)} + \frac{\varrho_2(1-\varrho_1)}{\mathtt{B}^*(\varrho_1)}\right]^n \varphi_3^n\,\|\mathrm{I}_1 - \mathrm{I}\|\,, \\ \|Z_{4_n}(t)\| &\leq \left[\frac{\varrho_1\varrho_2\Gamma(\varrho_2)}{\mathtt{B}^*(\varrho_1)\Gamma(\varrho_1+\varrho_2)} + \frac{\varrho_2(1-\varrho_1)}{\mathtt{B}^*(\varrho_1)}\right]^n \varphi_4^n\|\,\mathrm{R}_1 - \mathrm{R}\,\|. \end{aligned}$$

When $n \to \infty$, then $Z_{i_n}\left(t_{i_n} \to 0, i \in \mathbb{N}^4\right.$, for $\varphi_i < 1, (i = 1, \ldots, 4)$. Ultimately, the FF pneumonia system (2) has a solution.

5. Uniqueness of the model solutions

Lemma 3. *Model (2) has a unique solution if the inequality is satisfied:*

$$\Big(\frac{\varrho_2(1-\varrho_1)}{\mathtt{B}^*(\varrho_1)} + \frac{\varrho_1\varrho_2\Gamma(\varrho_2)}{\mathtt{B}^*(\varrho_1)\Gamma(\varrho_1+\varrho_2)}\Big)\varphi_i \leq 1, \quad \textit{for} \quad i = 1, 2, 3, 4.$$

Proof. Suppose that there is another solution to the fractal-fractional epidemiological model (2), and we can compute the value for $\tilde{\mathrm{S}}(\mathrm{t}), \tilde{\mathrm{C}}(\mathrm{t}), \tilde{\mathrm{I}}(\mathrm{t}), \tilde{\mathrm{R}}(\mathrm{t})$ using that solution, so that the value for

$$\tilde{S}(\mathtt{t}) = \frac{\varrho_2(1-\varrho_1)t^{\varrho_2-1}}{\mathtt{B}^*(\varrho_1)}W_1(\mathtt{t},\tilde{S}(\mathtt{t})) + \frac{\varrho_1\varrho_2}{\mathtt{B}^*(\varrho_1)\Gamma(\varrho_1)}\int_0^t \epsilon^{\varrho_2-1}(\mathtt{t}-\epsilon)^{\varrho_1-1}W_1(\epsilon,\tilde{S}(\epsilon))d\epsilon,$$
$$\tilde{C}(\mathtt{t}) = \frac{\varrho_2(1-\varrho_1)t^{\varrho_2-1}}{\mathtt{B}^*(\varrho_1)}W_2(\mathtt{t},\tilde{C}(\mathtt{t})) + \frac{\varrho_1\varrho_2}{\mathtt{B}^*(\varrho_1)\Gamma(\varrho_1)}\int_0^t \epsilon^{\varrho_2-1}(\mathtt{t}-\epsilon)^{\varrho_1-1}W_2(\epsilon,\tilde{C}(\epsilon))d\epsilon,$$
$$\tilde{I}(\mathtt{t}) = \frac{\varrho_2(1-\varrho_1)t^{\varrho_2-1}}{\mathtt{B}^*(\varrho_1)}W_3(\mathtt{t},\tilde{I}(\mathtt{t})) + \frac{\varrho_1\varrho_2}{\mathtt{B}^*(\varrho_1)\Gamma(\varrho_1)}\int_0^t \epsilon^{\varrho_2-1}(\mathtt{t}-\epsilon)^{\varrho_1-1}W_3(\epsilon,\tilde{I}(\epsilon))d\epsilon,$$
$$\tilde{R}(\mathtt{t}) = \frac{\varrho_2(1-\varrho_1)t^{\varrho_2-1}}{\mathtt{B}^*(\varrho_1)}W_4(\mathtt{t},\tilde{R}(\mathtt{t})) + \frac{\varrho_1\varrho_2}{\mathtt{B}^*(\varrho_1)\Gamma(\varrho_1)}\int_0^t \epsilon^{\varrho_2-1}(\mathtt{t}-\epsilon)^{\varrho_1-1}W_4(\epsilon,\tilde{R}(\epsilon))d\epsilon.$$

Here, we take the norm of the difference between $\mathrm{S}(\mathtt{t})$ and $\tilde{S}(\mathtt{t})$ as the difference between pair $\mathrm{S}(\mathtt{t})$ and $\tilde{S}(\mathtt{t})$ as follows:

$$\begin{aligned}
\|\,\mathrm{S}(\mathtt{t}) - \tilde{S}(\mathtt{t})\| &= \|\frac{\varrho_2(1-\varrho_1)t^{\varrho_2-1}}{\mathtt{B}^*(\varrho_1)}(W_1(\mathtt{t},\mathrm{S}(\mathtt{t})) - W_1(\mathtt{t},\tilde{S}(\mathtt{t})))\\
&\quad + \frac{\varrho_1\varrho_2}{\mathtt{B}^*(\varrho_1)\Gamma(\varrho_1)}\int_0^t \epsilon^{\varrho_2-1}(\mathtt{t}-\epsilon)^{\varrho_1-1}(W_1(\epsilon,S(\epsilon)) - W_1(\epsilon,\tilde{S}(\epsilon)))d\epsilon\|\\
&\le \frac{\varrho_2(1-\varrho_1)t^{\varrho_2-1}}{\mathtt{B}^*(\varrho_1)}\|W_1(\mathtt{t},\mathrm{S}(\mathtt{t})) - W_1(\mathtt{t},\tilde{S}(\mathtt{t}))\|\\
&\quad + \frac{\varrho_1\varrho_2}{\mathtt{B}^*(\varrho_1)\Gamma(\varrho_1)}\int_0^t \epsilon^{\varrho_2-1}(\mathtt{t}-\epsilon)^{\varrho_1-1}\|W_1(\epsilon,S(\epsilon)) - W_1(\epsilon,\tilde{S}(\epsilon))\|d\epsilon\\
&\le \frac{\varrho_2(1-\varrho_1)t_2-1}{\mathtt{B}^*(\varrho_1)}\varphi_1\|S-\tilde{S}\|\\
&\quad + \frac{\varrho_1\varrho_2}{\mathtt{B}^*(\varrho_1)\Gamma(\varrho_1)}\int_0^t \epsilon^{\varrho_2-1}(\mathtt{t}-\epsilon)^{\varrho_1-1}\varphi_1\|S-\tilde{S}\|d\epsilon\\
&\le \Big(\frac{\varrho_2(1-\varrho_1)}{\mathtt{B}^*(\varrho_1)} + \frac{\varrho_1\varrho_2\Gamma(\varrho_2)}{\mathtt{B}^*(\varrho_1)\Gamma(\varrho_1+\varrho_2)}\Big)\varphi_1\|S-\tilde{S}\|.
\end{aligned}$$

The inequality above can be further simplified in the following way:

$$\Big[1 - \Big(\frac{\varrho_2(1-\varrho_1)}{\mathtt{B}^*(\varrho_1)} + \frac{\varrho_1\varrho_2\Gamma(\varrho_2)}{\mathtt{B}^*(\varrho_1)\Gamma(\varrho_1+\varrho_2)}\Big)\varrho_1\Big]\|S-\tilde{S}\| \le 0.$$

Based on this inequality, we can write that $\|S-\tilde{S}\| = 0$. It then follows that $S = \tilde{S}$. Similarly, one can obtain $C = \tilde{C}$, $I = \tilde{I}$, and $R = \tilde{R}$ by repeating this process. This completes the proof.

6. Stability Analysis

When $I = C = 0$, one obtains the disease-free equilibrium point $E_0 = (\frac{\Pi}{\mu}, 0, 0, 0)$. For $\mathrm{I}^* > 0$, and taking ${}^{\mathtt{FF-AB}}\mathscr{D}_t^{\varrho_1,\varrho_2}\,\mathrm{S}(\mathtt{t}) = 0$, ${}^{\mathtt{FF-AB}}\mathscr{D}_t^{\varrho_1,\varrho_2}\,\mathrm{C}(\mathtt{t}) = 0$, ${}^{\mathtt{FF-AB}}\mathscr{D}_t^{\varrho_1,\varrho_2}\,\mathrm{I}(\mathtt{t}) = 0$,

$^{\mathtt{FF-AB}}\mathscr{D}_t^{\varrho_1,\varrho_2}\,\mathrm{R}(\mathtt{t})=0$. With $\ell_1=\frac{\vartheta\pi+(1-\vartheta)(\pi+\beta+\mu)}{(\mu+\tau+\sigma)}$, one obtains the endemic equilibrium point $\mathrm{E}^*=(\mathrm{S}^*,\mathrm{C}^*,\mathrm{I}^*,\mathrm{R}^*)$, with $\mathrm{S}^*=\frac{N(\pi+\beta+\mu)}{\ell_1+\varpi},\mathrm{C}^*=\frac{(\mu+\eta)(\Pi(\ell_1+\varpi)-\mu N(\pi+\beta+\mu))}{(\ell_1+\varpi)(\delta(\pi+\beta+\mu)(\mu+\eta)-\eta(\varrho_2+\tau\ell_1))}$, $\mathrm{I}^*=\frac{\ell_1(\mu+\eta)(\Pi(\ell_1+\varpi)-\mu N(\pi+\beta+\mu))}{(\ell_1+\varpi)(\delta(\pi+\beta+\mu)(\mu+\eta)-\eta(\varrho_2+\tau\ell_1))}$, $\mathrm{R}^*=\frac{(\varrho_2+\tau\ell_1)(\Pi(\ell_1+\varpi)-\mu N(\pi+\beta+\mu))}{(\ell_1+\varpi)(\delta(\pi+\beta+\mu)(\mu+\eta)-\eta(\varrho_2+\tau\ell_1))}$. According to [53], the basic reproduction number of the fractal-fractional model (2) is

$$\mathscr{R}_0=\frac{(\varpi\vartheta(\mu+\tau+\sigma)+(1-\vartheta)((\pi\varpi+(\pi+\beta+\mu)))\delta\,\mathrm{S}_0}{N(\pi+\beta+\mu)(\mu+\tau+\sigma)}.$$

Hence according to the Routh-Hurwitz criteria and as in [62], we have two cases:

(i) The pneumonia trivial equilibrium, denoted by $\mathrm{E}_0=(0,0,0,0)$, is stable locally asymptoticallyin if $\mathscr{R}_0<1$, but it is unstable if $\mathscr{R}_0>1$.

(ii) The equilibrium point $E_1=(\frac{\Pi}{\mu},0,0,0)$ of the nonlinear Atangana-Baleanu fractal-fractional SCIR model (2) is locally asymptotically stable if $\mathscr{R}_0<1$.

(iii) The equilibrium point $E_2=(\mathrm{S}^*,\mathrm{C}^*,\mathrm{I}^*,\mathrm{R}^*)$ of the nonlinear Atangana-Baleanu fractal-fractional SCIR model (2) is locally asymptotically stable if $\mathscr{R}_0>1$.

Definition 3 ([63], [64])**.** *Model (2) is Hyers-Ulam stable if $v_i>0$ for $i\in N_i^4$, satisfying for every $\delta_i, i\in N_i^4$*

$$|\,\mathrm{S}(\mathtt{t})-\frac{\varrho_2(1-\varrho_1)t^{\varrho_2-1}}{\mathtt{B}^*(\varrho_1)}W_1(\mathtt{t},\mathrm{S}(\mathtt{t}))-\frac{\varrho_1\varrho_2}{\mathtt{B}^*(\varrho_1)\Gamma(\varrho_1)}\int_0^t\epsilon^{\varrho_2-1}(\mathtt{t}-\epsilon)^{\varrho_1-1}W_1(\epsilon,S(\epsilon))d\epsilon|\le\delta_1,$$

$$|\,\mathrm{C}(\mathtt{t})-\frac{\varrho_2(1-\varrho_1)t^{\varrho_2-1}}{\mathtt{B}^*(\varrho_1)}W_2(\mathtt{t},\mathrm{C}(\mathtt{t}))-\frac{\varrho_1\varrho_2}{\mathtt{B}^*(\varrho_1)\Gamma(\varrho_1)}\int_0^t\epsilon^{\varrho_2-1}(\mathtt{t}-\epsilon)^{\varrho_1-1}W_2(\epsilon,C(\epsilon))d\epsilon|\le\delta_2,$$

$$|\,\mathrm{I}(\mathtt{t})-\frac{\varrho_2(1-\varrho_1)t^{\varrho_2-1}}{\mathtt{B}^*(\varrho_1)}W_3(\mathtt{t},\mathrm{I}(\mathtt{t}))-\frac{\varrho_1\varrho_2}{\mathtt{B}^*(\varrho_1)\Gamma(\varrho_1)}\int_0^t\epsilon^{\varrho_2-1}(\mathtt{t}-\epsilon)^{\varrho_1-1}W_3(\epsilon,I(\epsilon))d\epsilon|\le\delta_3,$$

$$|\,\mathrm{R}(\mathtt{t})-\frac{\varrho_2(1-\varrho_1)t^{\varrho_2-1}}{\mathtt{B}^*(\varrho_1)}W_4(\mathtt{t},\mathrm{R}(\mathtt{t}))-\frac{\varrho_1\varrho_2}{\mathtt{B}^*(\varrho_1)\Gamma(\varrho_1)}\int_0^t\epsilon^{\varrho_2-1}(\mathtt{t}-\epsilon)^{\varrho_1-1}W_4(\epsilon,R(\epsilon))d\epsilon|\le\delta_4.$$

Several approximate solutions $(\mathrm{S}_1(\mathtt{t}),\mathrm{C}_1(\mathtt{t}),\mathrm{I}_1(\mathtt{t}),\mathrm{R}_1(\mathtt{t}))$ to the model problem (2) are available, with the following integral equations satisfying their terms

$$\mathrm{S}_1(\mathtt{t})=\frac{\varrho_2(1-\varrho_1)t^{\varrho_2-1}}{\mathtt{B}^*(\varrho_1)}W_1(\mathtt{t},\mathrm{S}_1(\mathtt{t}))+\frac{\varrho_1\varrho_2}{\mathtt{B}^*(\varrho_1)\Gamma(\varrho_1)}\int_0^t\epsilon^{\varrho_2-1}(\mathtt{t}-\epsilon)^{\varrho_1-1}W_1(\epsilon,\mathrm{S}_1(\epsilon))d\epsilon$$

$$\mathrm{C}_1(\mathtt{t})=\frac{\varrho_2(1-\varrho_1)t^{\varrho_2-1}}{\mathtt{B}^*(\varrho_1)}W_2(\mathtt{t},\mathrm{C}_1(\mathtt{t}))+\frac{\varrho_1\varrho_2}{\mathtt{B}^*(\varrho_1)\Gamma(\varrho_1)}\int_0^t\epsilon^{\varrho_2-1}(\mathtt{t}-\epsilon)^{\varrho_1-1}W_2(\epsilon,\mathrm{C}_1(\epsilon))d\epsilon,$$

$$\mathrm{I}_1(\mathtt{t})=\frac{\varrho_2(1-\varrho_1)t^{\varrho_2-1}}{\mathtt{B}^*(\varrho_1)}W_1(\mathtt{t},\mathrm{S}_1(\mathtt{t}))+\frac{\varrho_1\varrho_2}{\mathtt{B}^*(\varrho_1)\Gamma(\varrho_1)}\int_0^t\epsilon^{\varrho_2-1}(\mathtt{t}-\epsilon)^{\varrho_1-1}W_3(\epsilon,\mathrm{I}_1(\epsilon))d\epsilon,$$

$$\mathrm{R}_1(\mathtt{t})=\frac{\varrho_2(1-\varrho_1)t^{\varrho_2-1}}{\mathtt{B}^*(\varrho_1)}W_4(\mathtt{t},\mathrm{R}_1(\mathtt{t}))+\frac{\varrho_1\varrho_2}{\mathtt{B}^*(\varrho_1)\Gamma(\varrho_1)}\int_0^t\epsilon^{\varrho_2-1}(\mathtt{t}-\epsilon)^{\varrho_1-1}W_4(\epsilon,\mathrm{R}_1(\epsilon))d\epsilon,$$

such that

$$\begin{aligned}|\,\mathrm{S}(\mathtt{t})-\mathrm{S}_1(\mathtt{t})|&\le\tau_1\delta_1,\\ |\,\mathrm{I}(\mathtt{t})-\mathrm{I}_1(\mathtt{t})|&\le\tau_2\delta_2,\\ |\,\mathrm{S}(\mathtt{t})-\mathrm{S}_1(\mathtt{t})|&\le\tau_3\delta_3,\\ |\,\mathrm{I}(\mathtt{t})-\mathrm{I}_1(\mathtt{t})|&\le\tau_4\delta_4.\end{aligned}\tag{4}$$

Theorem 1. *If (4) is true, then model (2) satisfies the Hyers-Ulam Stability condition.*

Proof. Based on the results of Lemma 1, we can conclude the following:

$$\begin{aligned}
|\,\mathrm{S}(\mathtt{t})-\mathrm{S}_1(\mathtt{t})| &= \Big|\frac{\varrho_2(1-\varrho_1)t^{\varrho_2-1}}{\mathtt{B}^*(\varrho_1)}(W_1(\mathtt{t},\mathrm{S}(\mathtt{t}))-W_1(\mathtt{t},\mathrm{S}_1(\mathtt{t})))\\
&\quad+\frac{\varrho_1\varrho_2}{\mathtt{B}^*(\varrho_1)\Gamma(\varrho_1)}\int_0^t\epsilon^{\varrho_2-1}(\mathtt{t}-\epsilon)^{\varrho_1-1}(W_1(\epsilon,S(\epsilon))-W_1(\epsilon,\mathrm{S}_1(\epsilon)))d\epsilon\Big|\\
&\le\frac{\varrho_2(1-\varrho_1)t^{\varrho_2-1}}{\mathtt{B}^*(\varrho_1)}\eta_1\|S-\mathrm{S}_1\|\\
&\quad+\frac{\varrho_1\varrho_2}{\mathtt{B}^*(\varrho_1)\Gamma(\varrho_1)}\int_0^t\epsilon^{\varrho_2-1}(\mathtt{t}-\epsilon)^{\varrho_1-1}\eta_1\|S-\mathrm{S}_1\|d\epsilon\\
&\le\Big(\frac{\varrho_2(1-\varrho_1)}{\mathtt{B}^*(\varrho_1)}+\frac{\varrho_1\varrho_2\Gamma(\varrho_2)}{\mathtt{B}^*(\eta_1)\Gamma(\varrho_1+\varrho_2)}\Big)\eta_1\|S-\mathrm{S}_1\|.
\end{aligned}$$

Now, let $\eta_1=\delta_1,\Big(\frac{\varrho_2(1-\varrho_1)}{\mathtt{B}^*(\varrho_1)}+\frac{\varrho_1\varrho_2\Gamma(\varrho_2)}{\mathtt{B}^*(\varrho_1)\Gamma(\varrho_1+\varrho_2)}\Big)\|S-\mathrm{S}_1\|=\tau_1$. Then we have

$$|\,\mathrm{S}(\mathtt{t})-\mathrm{S}_1(\mathtt{t})|\le\tau_1\delta_1.$$

Similarly, one obtains

$$|\,\mathrm{C}(\mathtt{t})-\mathrm{C}_1(\mathtt{t})|\le\tau_2\delta_2,$$

with $\eta_2=\delta_2,\Big(\frac{\varrho_2(1-\varrho_1)}{\mathtt{B}^*(\varrho_1)}+\frac{\varrho_1\varrho_2\Gamma(\varrho_2)}{\mathtt{B}^*(\varrho_1)\Gamma(\varrho_1+\varrho_2)}\Big)\|C-\mathrm{C}_1\|=\tau_2$.

Also

$$|\,\mathrm{I}(\mathtt{t})-\mathrm{I}_1(\mathtt{t})|\le\tau_3\delta_3,$$

with $\eta_3=\delta_3,\Big(\frac{\varrho_2(1-\varrho_1)}{\mathtt{B}^*(\varrho_1)}+\frac{\varrho_1\varrho_2\Gamma(\varrho_2)}{\mathtt{B}^*(\varrho_1)\Gamma(\varrho_1+\varrho_2)}\Big)\|\,\mathrm{I}-\mathrm{I}_1\|=\tau_3$.

Also

$$|\,\mathrm{R}(\mathtt{t})-\mathrm{R}_1(\mathtt{t})|\le\tau_4\delta_4,$$

with $\eta_4=\delta_4,\Big(\frac{\varrho_2(1-\varrho_1)}{\mathtt{B}^*(\varrho_1)}+\frac{\varrho_1\varrho_2\Gamma(\varrho_2)}{\mathtt{B}^*(\varrho_1)\Gamma(\varrho_1+\varrho_2)}\Big)\|R-\mathrm{R}_1\|=\tau_4$.

7. Fractal-fractional Atangana-Baleanu Scheme

The Antangana-Baleanu integral gives us

$$\Psi(\mathtt{t})=\Psi(0)+\frac{1-\varrho_1}{\hbar(\varrho_1)}\Xi(\mathtt{t},\Psi(\mathtt{t}))+\frac{\varrho_1}{\hbar(\varrho_1)\Gamma(\varrho_1)}\int_0^{\mathtt{t}}(\mathtt{t}-\epsilon)^{\varrho_1-1}\epsilon^{\varrho_2-1}\Xi(\epsilon,\Psi(\epsilon))d\epsilon.$$

Replacing $\mathtt{t}$ by $\mathtt{t}_{n+1}$ we have

$$\Psi^{n+1}=\Psi(0)+\frac{1-\varrho_1}{\hbar(\varrho_1)}\Xi\left(\mathtt{t}_{n+1},\Psi(\mathtt{t})\right)+\frac{\varrho_1}{\hbar(\varrho_1)\Gamma(\varrho_1)}\int_0^{\mathtt{t}_{n+1}}\left(\mathtt{t}_{n+1}-\epsilon\right)^{\varrho_1-1}\epsilon^{\varrho_2-1}\Xi(\epsilon,\Psi(\epsilon))d\epsilon.$$

Application of the two-step Lagrange polynomial yields

$$\begin{aligned}\Xi(\mathtt{t},(y,\Psi(\mathtt{t}))&=\frac{(y-\mathtt{t}_{\epsilon-1})\,\Xi(\mathtt{t},(\mathtt{t}_{\epsilon},\Psi\,(\mathtt{t}_{\epsilon}))}{\mathtt{t}_{\epsilon}-\mathtt{t}_{\epsilon-1}}-\frac{(y-\mathtt{t}_{\epsilon})\,\Xi\,(\mathtt{t}_{\epsilon-1},\Psi\,(\mathtt{t}_{\epsilon-1})}{\mathtt{t}_{\epsilon}-\mathtt{t}_{\epsilon-1}}\\&=\frac{\Xi(\mathtt{t},(\mathtt{t}_{\epsilon},\Psi\,(\mathtt{t}_{\epsilon}))\,(x-\mathtt{t}_{\epsilon-1})}{\mathtt{t}_{\epsilon}-\mathtt{t}_{\epsilon-1}}-\frac{\Xi\,(\mathtt{t}_{\epsilon-1},\Psi\,(\mathtt{t}_{\epsilon-1})\,(y-\mathtt{t}_{\epsilon})}{\mathtt{t}_{\epsilon}-\mathtt{t}_{\epsilon-1}}\\&=\frac{\Xi(\mathtt{t},(\mathtt{t}_{\epsilon},\Psi\,(\mathtt{t}_{\epsilon}))\,(y-\mathtt{t}_{\epsilon-1})}{h}-\frac{\Xi\,(\mathtt{t}_{\epsilon-1},\Psi\,(\mathtt{t}_{\epsilon-1})\,(y-\mathtt{t}_{\epsilon})}{h}.\end{aligned}$$

Using the Lagrange polynomial, we obtain

$$\begin{aligned}\Psi^{n+1}&=\Psi(0)+\frac{1-\varrho_1}{\hbar(\varrho_1)}\Xi(\mathtt{t},(\mathtt{t}_n,\Psi\,(\mathtt{t}_n))\\&+\frac{\varrho_1}{\hbar(\varrho_1)\Gamma(\varrho_1)}\sum_{\epsilon=1}^{n}\left(\frac{\Xi(\mathtt{t},(\mathtt{t}_{\epsilon},\Psi\,(\mathtt{t}_{\epsilon}))}{h}\int_{\mathtt{t}_{\epsilon}}^{\mathtt{t}_{\epsilon}+1}(\epsilon-\mathtt{t}_{\epsilon}-1)\,(\mathtt{t}_{n+1}-\epsilon)^{\varrho_1-1}\,d\epsilon\right.\\&\left.-\frac{\Xi(\mathtt{t},(\mathtt{t}_{\epsilon-1},\Psi\,(\mathtt{t}_{\epsilon-1}))}{h}\int_{\mathtt{t}_{\epsilon}}^{\mathtt{t}_{n+1}}(\epsilon-\mathtt{t}_{\epsilon})\,(\mathtt{t}_{n+1}-\epsilon)^{\varrho_1-1}\,d\epsilon\right).\end{aligned}$$

Now solving the integral we get

$$\begin{aligned}\Psi^{n+1}&=\Psi(0)+\frac{1-\varrho_1}{\hbar(\varrho_1)}\Xi(\mathtt{t},(\mathtt{t}_n,\Psi\,(\mathtt{t}_n))+\frac{\varrho_1 h^{\varrho_1}}{\Gamma\,(\varrho_1+2)}\\&\times\sum_{\epsilon=1}^{n}\left[\Xi(\mathtt{t},(\mathtt{t}_{\epsilon},\Psi\,(\mathtt{t}_{\epsilon}))\left((n-\epsilon+1)^{\varrho_1}\,(n-\epsilon+2+\varrho_1)\;-(n-\epsilon)^{\varrho_1}\,(n-\epsilon+2+2\varrho_1)\right)\right.\\&\left.-\Xi(\mathtt{t},(\mathtt{t}_{\epsilon-1},\Psi_{\epsilon-1})\left((n-\epsilon+1)^{\varrho_1+1}-(n-\epsilon+1+\varrho_1)\,(n-\epsilon)^{\varrho_1}\right)\right].\end{aligned}$$

Now replacing the value of $\Xi(y,\Psi(\mathtt{t}))$ we get

$$\begin{aligned}\Psi^{n+1}&=\Psi(0)+\varrho_2\mathtt{t}^{\varrho_2-1}\frac{1-\varrho_1}{\hbar(\varrho_1)}\Upsilon\,(\mathtt{t}_{\epsilon},\Psi\,(\mathtt{t}_{\epsilon}))+\varrho_2\mathtt{t}^{\varrho_2-1}\frac{\varrho_1 h^{\varrho_1}}{\Gamma\,(\varrho_1+2)}\\&\times\sum_{\epsilon=1}^{n}\left[\Upsilon\,(\mathtt{t}_{\epsilon},\Psi\,(\mathtt{t}_{\epsilon}))\left((n+1-\epsilon)^{\varrho_1}\,(n-\epsilon+2+\varrho_1)\;-(n-\epsilon)^{\varrho_1}\,(n-\epsilon+2+2\varrho_1)\right)\right.\\&\left.-\Upsilon\,(\mathtt{t}_{\epsilon-1},\Psi_{\epsilon-1})\left((n-\epsilon+1)^{\varrho_1+1}-(n-\epsilon+1+\varrho_1)\,(n-\epsilon)^{\varrho_1}\right)\right].\end{aligned}$$

Therefore, the above system's numerical scheme is

$$\begin{aligned}\mathrm{S}^{n+1}&=\mathrm{S}(0)+\varrho_2\mathtt{t}^{\varrho_2-1}\frac{1-\varrho_1}{\hbar(\varrho_1)}W_1\,(\mathtt{t}_{\epsilon},\mathrm{S}\,(\mathtt{t}_{\epsilon}))+\varrho_2\mathtt{t}^{\varrho_2-1}\frac{\varrho_1 h^{\varrho_1}}{\Gamma\,(\varrho_1+2)}\\&\times\sum_{\epsilon=1}^{n}\left[W_1\,(\mathtt{t}_{\epsilon},\mathrm{S}\,(\mathtt{t}_{\epsilon}))\left((n-\epsilon+1)^{\varrho_1}\,(n-\epsilon+2+\varrho_1)\;-(n-\epsilon)^{\varrho_1}\,(n-\epsilon+2+2\varrho_1)\right)\right.\\&\left.-W_1\,(\mathtt{t}_{\epsilon-1},\mathrm{S}_{\epsilon-1})\left((n-\epsilon+1)^{\varrho_1+1}-(n-\epsilon+1+\varrho_1)\,(n-\epsilon)^{\varrho_1}\right)\right],\end{aligned}$$

$$
\begin{aligned}
\mathrm{C}^{n+1} &= \mathrm{C}(0) + \varrho_2 \mathtt{t}^{\varrho_2-1} \frac{1-\varrho_1}{\hbar(\varrho_1)} W_2\left(\mathtt{t}_\epsilon, \mathrm{C}\left(\mathtt{t}_\epsilon\right)\right) + \varrho_2 \mathtt{t}^{\varrho_2-1} \frac{\varrho_1 h^{\varrho_1}}{\Gamma\left(\varrho_1+2\right)} \\
&\times \sum_{\epsilon=1}^{n} \left[W_2\left(\mathtt{t}_\epsilon, \mathrm{C}\left(\mathtt{t}_\epsilon\right)\right)\left((n-\epsilon+1)^{\varrho_1}\left(n-\epsilon+2+\varrho_1\right) - (n-\epsilon)^{\varrho_1}\left(n-\epsilon+2+2\varrho_1\right)\right)\right. \\
&\left. - W_2\left(\mathtt{t}_{\epsilon-1}, \mathrm{C}_{\epsilon-1}\right)\left((n-\epsilon+1)^{\varrho_1+1} - \left(n-\epsilon+1+\varrho_1\right)(n-\epsilon)^{\varrho_1}\right)\right], \\
\mathrm{I}^{n+1} &= \mathrm{I}(0) + \varrho_2 \mathtt{t}^{\varrho_2-1} \frac{1-\varrho_1}{\hbar(\varrho_1)} W_3\left(\mathtt{t}_\epsilon, \mathrm{I}\left(\mathtt{t}_\epsilon\right)\right) + \varrho_2 \mathtt{t}^{\varrho_2-1} \frac{\varrho_1 h^{\varrho_1}}{\Gamma\left(\varrho_1+2\right)} \\
&\times \sum_{\epsilon=1}^{n} \left[W_3\left(\mathtt{t}_\epsilon, \mathrm{I}\left(\mathtt{t}_\epsilon\right)\right)\left((n-\epsilon+1)^{\varrho_1}\left(n-\epsilon+2+\varrho_1\right) - (n-\epsilon)^{\varrho_1}\left(n-\epsilon+2+2\varrho_1\right)\right)\right. \\
&\left. - W_3\left(\mathtt{t}_{\epsilon-1}, \mathrm{I}_{\epsilon-1}\right)\left((n-\epsilon+1)^{\varrho_1+1} - \left(n-\epsilon+1+\varrho_1\right)(n-\epsilon)^{\varrho_1}\right)\right], \\
\mathrm{R}^{n+1} &= \mathrm{R}(0) + \varrho_2 \mathtt{t}^{\varrho_2-1} \frac{1-\varrho_1}{\hbar(\varrho_1)} W_4\left(\mathtt{t}_\epsilon, \mathrm{R}\left(\mathtt{t}_\epsilon\right)\right) + \varrho_2 \mathtt{t}^{\varrho_2-1} \frac{\varrho_1 h^{\varrho_1}}{\Gamma\left(\varrho_1+2\right)} \\
&\times \sum_{\epsilon=1}^{n} \left[W_4\left(\mathtt{t}_\epsilon, \mathrm{R}\left(\mathtt{t}_\epsilon\right)\right)\left((n-\epsilon+1)^{\varrho_1}\left(n-\epsilon+2+\varrho_1\right) - (n-\epsilon)^{\varrho_1}\left(n-\epsilon+2+2\varrho_1\right)\right)\right. \\
&\left. - W_4\left(\mathtt{t}_{\epsilon-1}, \mathrm{R}_{\epsilon-1}\right)\left((n-\epsilon+1)^{\varrho_1+1} - \left(n-\epsilon+1+\varrho_1\right)(n-\epsilon)^{\varrho_1}\right)\right].
\end{aligned}
$$

7.1. Numerical Simulations and Discussion

Detailed computations of model (2) with a particular formulation are presented here. The numerical values are given from [62]: $S(0) = 0.9$, $C(0) = 0.2$, $I(0) = 0.3$, $R(0) = 0.1$. The following figures provide a numerical description of the model. Fig. 1 is a description of the numerical data for the $\mathrm{S}(\mathtt{t})$.

The numerical simulations presented in the figures highlight the impact of fractal-fractional operators on the dynamics of pneumonia transmission. The variations in the fractional orders demonstrate the flexibility and accuracy of the fractal-fractional approach in capturing different dynamical behaviors, as compared to the classical integer-order models.

In Figure 1, the dynamics of the susceptible population $S(t)$ show an initial increase, reflecting the recruitment rate into the susceptible class, followed by stabilization. This behavior is consistent across different fractional orders, emphasizing the robustness of the model in predicting long-term stability. This figure illustrates the evolution of the susceptible population over time for different fractional orders. The population initially increases due to recruitment into the susceptible class and then stabilizes. Higher fractional orders ($\alpha \approx 1$) exhibit behavior similar to classical models, whereas lower orders introduce stronger memory effects, altering the system's response. Figure 2 illustrates the behavior of the carrier population $C(t)$, which exhibits an early decline before stabilizing. This decline suggests that carriers either progress to the infected class or recover due to treatment or natural immunity. The rate of change is influenced by the fractional order, indicating the significance of memory effects in disease progression. The dynamics of carriers, who are infected but asymptomatic, are displayed. The carrier population declines over time,

indicating progression to the infected class or recovery. Lower fractional orders slow down the decline, showing the influence of memory effects on disease transmission. Figure shows the infected population $I(t)$, which initially increases before declining and stabilizing. The infected class dynamics are particularly sensitive to changes in fractional orders, as lower orders lead to faster stabilization. This result reflects the importance of fractional derivatives in modeling the memory and long-term effects of the infection process. The number of infected individuals initially rises, peaks, and then declines as people recover or die. Fractional models exhibit smoother transitions and prolonged infection durations compared to classical integer-order models. The choice of fractional order significantly affects the persistence of the disease within the population. The recovered population $R(t)$, depicted in Figure 4, increases significantly during the initial days before reaching stability. This trend aligns with the natural progression of recovery in the population. The stabilization of all compartments over time underlines the equilibrium behavior predicted by the model. The recovered population increases in the early stages and eventually stabilizes. Higher fractional orders lead to a quicker stabilization of the recovered class, whereas lower orders suggest prolonged memory effects and delayed recovery.

Figures 5–7 provide a comprehensive comparison of the solutions for all compartments under varying fractional orders. These figures demonstrate that as the fractional orders approach 1.0, the solutions converge to the classical case, validating the model's ability to replicate traditional integer-order dynamics while offering greater flexibility. These figures provide a comparative analysis of all compartments $(S(t), C(t), I(t), R(t))$ under varying fractional orders. As the fractional order approaches 1, the system's behavior aligns with classical integer-order models. Fractional models allow greater flexibility in capturing real-world disease dynamics, incorporating memory effects and population heterogeneity.

Overall, the results emphasize the utility of the fractal-fractional operators in accurately modeling complex real-world phenomena, such as pneumonia transmission. The ability to vary the fractional orders allows for a better understanding of the disease dynamics under different scenarios, including memory effects and heterogeneous population behaviors. These insights can be instrumental in optimizing intervention strategies, such as vaccination and treatment programs. Future work could focus on incorporating environmental and social factors, which play a critical role in the spread and treatment of pneumonia, to further enhance the model's applicability.

8. Conclusions

This study explored a pneumonia transmission model using fractal-fractional derivatives, demonstrating the utility of these operators in capturing disease spread dynamics. The numerical simulations revealed how varying the fractional orders influence the behavior of the model compartments, including susceptible, carrier, infected, and recovered populations. By incorporating long-memory effects and heterogeneous responses, the fractal-fractional model provides a more accurate and flexible framework than traditional integer-order models. The results showed that as fractional orders approach 1, the solutions converge to the classical case. As a result, fractional calculus is compatible

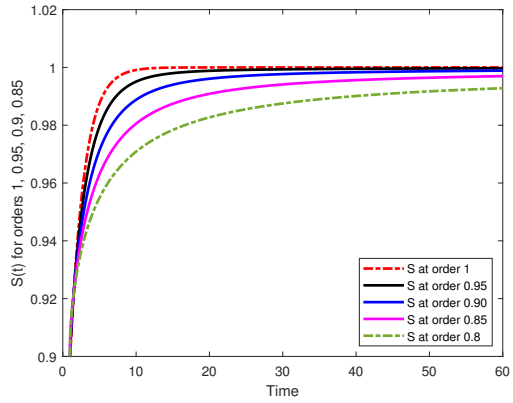

Figure 1: Susceptible class for the different fractional orders of the model (2).

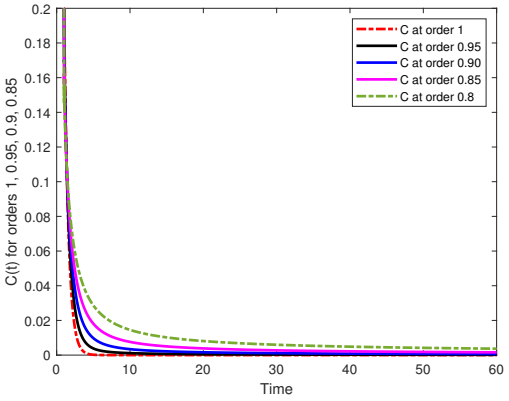

Figure 2: C(t) class for the different fractional orders of the model (2).

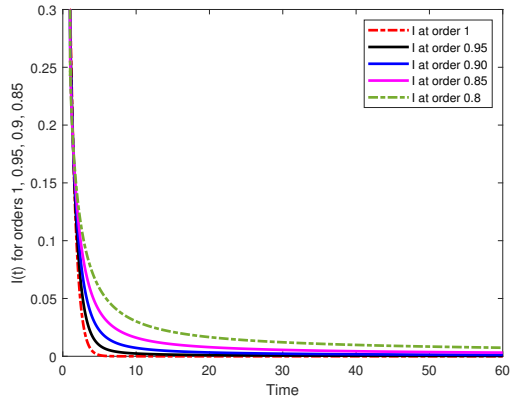

Figure 3: Infected class for the different fractional orders of the model (2).

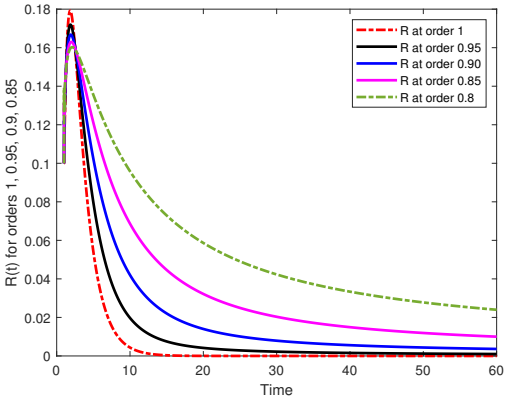

Figure 4: R(t) class for the different fractional orders of the model (2).

with conventional approaches. The stabilization of all compartments over time indicates equilibrium points and supports the model's effectiveness in predicting disease dynamics.

This study emphasizes the importance of fractional-order modeling in understanding real-world phenomena like pneumonia transmission. By adjusting fractional orders, the model can account for diverse population behaviors. This offers valuable insights into the effects of interventions such as vaccination and treatment strategies. Future work should consider environmental and social factors, such as air quality, temperature, and population density. This will further refine the model and enhance its applicability. The proposed method could also be compared with other numerical schemes for a deeper understanding of its robustness and computational efficiency. The fractal-fractional approach has significant potential for improving disease modeling and public health decisions.

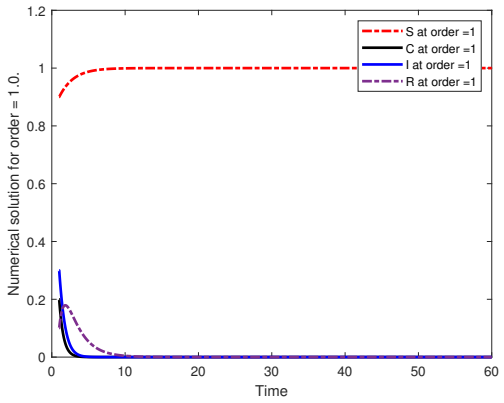

Figure 5: Time series of S(t), C(t), I(t), and R(t) using fractal fractional methods in the sense of Atangana-Baleanu operators for $\varrho_1 = 1, \varrho_2 = 1$.

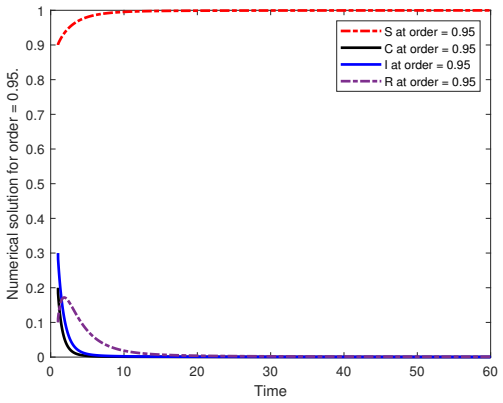

Figure 6: Time series of S(t), C(t), I(t), and R(t) using fractal fractional methods in the sense of Atangana-Baleanu operators for $\varrho_1 = 0.95, \varrho_2 = 0.95$.

Π	the recruitment rate into susceptible population per capita	0.5
δ	the rate of transmission	2.5
ϖ	represents the rate of treated individuals having vaccinated	0.1124
μ	the natural mortality rate of individuals per capita	0.5
η	Average time symptomatic infectious have symptoms	0.00641
m	the recovery rate of carriers per capita	0.515
π	the rate of developing symptoms by carriers	0.7096
ϑ	the proportion of susceptible individuals who joins the carriers	0.563
τ	the recovery rate of individuals who are infected of Pneumonia per capita	0.641
σ	Birth rate per capita of the human population affected by disease	0.53

Table 1: The values of parameters and initial populations in this study are obtained from the WHO situation report (the National Health Commission of the Republic of China) presented in [62]. https://doi.org/10.32604/cmc.2022.020732

Acknowledgment

The authors extend their appreciation to Umm Al-Qura University, Saudi Arabia for funding this research work through grant number: 25UQU4220004GSSR02.

Funding

This research work was funded by Umm Al-Qura University, Saudi Arabia under grant number: 25UQU4220004GSSR02.

Data Availability

All data is included in the manuscript. https://doi.org/10.32604/cmc.2022.020732

References

[1] J. Ong'ala, P. Oleche, and J.Y.T. Mugisha. Mathematical model for pneumonia dynamics with carriers. *Int. J. Math. Anal.*, 7(50):2457–2473, 2013.

[2] E. Mochan, D. Swigon, G. Ermentrout, S. Luken, and G.A. Clermont. Mathematical model of intrahost pneumococcal pneumonia infection dynamics in murine strains. *J. Theor. Biol.*, 353:44–54, 2014.

[3] G.L. Drusano, W. Liu, S. Fikes, R. Cirz, N. Robbins, S. Kurhanewicz, and A. Louie. Interaction of drug- and granulocyte-mediated killing of pseudomonas aeruginosa in a murine pneumonia model. *J. Infect. Dis.*, 210(8):1319–1324, 2014.

[4] E.J. Ndelwa, M. Kgosimore, E.S. Massawe, and L. Namkinga. Mathematical modelling and analysis of treatment and screening of pneumonia. *Math. Theory Model.*, 5(10):21–39, 2015.

[5] K. Kosasih, U.R. Abeyratne, V. Swarnkar, and R. Triasih. Wavelet augmented cough analysis for rapid childhood pneumonia diagnosis. *IEEE Trans. Biomed. Eng.*, 62(4):1185–1194, 2015.

[6] A.C.G. César, L.F.C. Nascimento, K.C.C. Mantovani, and L.C.P. Vieira. Fine particulate matter estimated by mathematical model and hospitalisations for pneumonia and asthma in children. *Rev. Paul. Pediatr. (Engl. Ed.)*, 34(1):18–23, 2016.

[7] C. Marchello, A.P. Dale, T.N. Thai, D.S. Han, and M.H. Ebell. Prevalence of atypical pathogens in patients with cough and community-acquired pneumonia: a meta-analysis. *Ann. Fam. Med.*, 14(6):552–566, 2016.

[8] Y.H. Cheng, S.H. You, Y.J. Lin, S.C. Chen, W.Y. Chen, W.C. Chou, and C.M. Liao. Mathematical modeling of post coinfection with influenza a virus and streptococcus pneumoniae, with implications for pneumonia and copd-risk assessment. *Int. J. Chronic Obstr. Pulm. Dis.*, 12:1973–1988, 2017.

[9] K. Kosasih and U. Abeyratne. Exhaustive mathematical analysis of simple clinical measurements for childhood pneumonia diagnosis. *World J. Pediatr.*, 13(5):446–456, 2017.

[10] G.T. Tilahun, O.D. Makinde, and D. Malonza. Modelling and optimal control of pneumonia disease with cost-effective strategies. *J. Biol. Dyn.*, 11(2):400–426, 2017.

[11] G.T. Tilahun, O.D. Makinde, and D. Malonza. Co-dynamics of pneumonia and typhoid fever diseases with cost-effective optimal control analysis. *Appl. Math. Comput.*, 316:438–459, 2018.

[12] M. Raj, M. Reddy, M. Mufeed, and S. Karthika. Hmm based cough sound analysis for classifying asthma and pneumonia in paediatric population. *International Journal of Pure and Applied Mathematics*, 118(18):609–616, 2018.

[13] M. Kizito and J. Tumwiine. A mathematical model of treatment and vaccination interventions of pneumococcal pneumonia infection dynamics. *Journal of Applied Mathematics*, 2018.

[14] F.K. Mbabazi, J.Y.T. Mugisha, and M. Kimathi. Modeling the within-host coinfection of influenza a virus and pneumococcus. *Applied Mathematics and Computation*, 339:488–506, 2018.

[15] G.T. Tilahun. Optimal control analysis of pneumonia and meningitis coinfection. *Computational and Mathematical Methods in Medicine*, pages 1–15, 2019.

[16] G.T. Tilahun. Modeling co-dynamics of pneumonia and meningitis diseases. *Advances in Differential Equations*, 2019(1):1, 2019.

[17] I.M. Diah and N. Aziz. Stochastic modelling for pneumonia incidence: a conceptual framework. In *AIP Conference Proceedings*, volume 1, pages 1–3. AIP, New York, 2019.

[18] F.K. Mbabazi, J.Y. Mugisha, and M. Kimathi. Hopf-bifurcation analysis of pneumococcal pneumonia with time delays. *Abstract and Applied Analysis*, 2019(1):1, 2019.

[19] D. Otoo, P. Opoku, S. Charles, and A.P. Kingsley. Deterministic epidemic model for (svcsycasyir) pneumonia dynamics, with vaccination and temporal immunity. *Infectious Disease Modelling*, 5:42–60, 2020.

[20] O.C. Zephaniah, U.I.R. Nwaugonma, I.S. Chioma, and O. Adrew. A mathematical model and analysis of an sveir model for streptococcus pneumonia with saturated incidence force of infection. *Mathematical Modelling and Applications*, 5(1):16, 2020.

[21] W.K. Ming, J. Huang, and C.J. Zhang. Breaking down of healthcare system: mathematical modelling for controlling the novel coronavirus (2019-ncov) outbreak in wuhan, china. *BioRxiv*, 1:1–18, 2020.

[22] S.M. Jung, R. Kinoshita, R.N. Thompson, N.M. Linton, Y. Yang, A.R. Akhmetzhanov, and H. Nishiura. Epidemiological identification of a novel pathogen in real-time: analysis of the atypical pneumonia outbreak in wuhan, china, 2019—2020. *Journal of Clinical Medicine*, 9(3):1–18, 2020.

[23] N.M. Wafula, B.O. Kwach, and V.N. Marani. Mathematical modeling and optimal control for controlling pneumonia-hiv coinfection. *International Journal of Innovative Research and Development*, 10(1):138–144, 2021.

[24] K.I. Ouwatobi and L.M. Erinle-Ibrahim. Mathematical modeling of pneumonia dynamics of children under the age of five. *Research Square*, 1:1–16, 2021.

[25] Sayed Saber, Azza M. Alghamdi, Ghada A. Ahmed, and Khulud M. Alshehri. Mathematical modelling and optimal control of pneumonia disease in sheep and goats in al-baha region with cost-effective strategies. *AIMS Mathematics*, 7(7):12011–12049, 2022.

[26] N. Almutairi, S. Saber, and A. Hijaz. The fractal-fractional atangana-baleanu operator for pneumonia disease: stability, statistical and numerical analyses. *AIMS Mathematics*, 8(12):29382–29410, 2023.

[27] Muhammad Naveed, Dumitru Baleanu, Ali Raza, et al. Modeling the transmission dynamics of delayed pneumonia-like diseases with a sensitivity of parameters. *Advances in Difference Equations*, 2021:468, 2021.

[28] H. Jafari, H. K. Jassim, and J. Vahidi. Reduced differential transform and variational iteration methods for 3d diffusion model in fractal heat transfer within local fractional operators. *Thermal Science*, 22:S301–S307, 2018.

[29] D. Baleanu and H. K. Jassim. A modification fractional homotopy perturbation method for solving helmholtz and coupled helmholtz equations on cantor sets. *Fractal*

and Fractional, 3(30):1–8, 2019.

[30] Y. Chatibi, E.H. El Kinani, and A. Ouhadan. Variational calculus involving nonlocal fractional derivative with mittag–leffler kernel. *Chaos, Solitons & Fractals*, 118:117–121, 2019.

[31] Y. Chatibi. Analytical solutions of virus propagation model in blockchain networks. *Quaestiones Mathematicae*, 47(11):2153–2161, 2024.

[32] P. Arena, R. Caponetto, L. Fortuna, and D. Porto. *Nonlinear Noninteger Order Circuits and Systems*. World Scientific, Singapore, 2000.

[33] K. S. Nisar, M. Farman, M. Abdel-Aty, and C. Ravichandran. A review of fractional-order models for plant epidemiology. *Progr. Fract. Differ. Appl.*, 10:489–521, 2024.

[34] E. Ahmed and A. S. Elgazzar. On fractional order differential equations model for nonlocal epidemics. *Physica A*, 379:607–614, 2007.

[35] W. Li, Y. Wang, J. Cao, and M. Abdel-Aty. Dynamics and backward bifurcations of sei tuberculosis models in homogeneous and heterogeneous populations. *J. Math. Anal. Appl.*, 543:128924, 2025.

[36] K. S. Nisar, M. Farman, M. Abdel-Aty, and C. Ravichandran. A review of fractional order epidemic models for life sciences problems: Past, present and future. *Alexandria Eng. J.*, 95:283–305, 2024.

[37] R. Hilfer. *Applications of Fractional Calculus in Physics*. World Scientific, Singapore, 2000.

[38] S. Saber. Control of chaos in the burke-shaw system of fractal-fractional order in the sense of caputo-fabrizio. *J. Appl. Math. Comput. Mech.*, 23:83–96, 2024.

[39] T. Yan et al. Analysis of a lorenz model using adomian decomposition and fractal-fractional operators. *Thermal Sci.*, 8(6B):5001–5009, 2024.

[40] A. Alsulami et al. Controlled chaos of a fractal–fractional newton-leipnik system. *Thermal Sci.*, 28(6B):5153–5160, 2024.

[41] M. Alhazmi et al. Numerical approximation method and chaos for a chaotic system in sense of caputo-fabrizio operator. *Thermal Sci.*, 28(6B):5161–5168, 2024.

[42] N. Almutairi and S. Saber. Existence of chaos and the approximate solution of the lorenz–lü–chen system with the caputo fractional operator. *AIP Adv.*, 14:015112, 2024.

[43] N. Almutairi and S. Saber. On chaos control of nonlinear fractional newton-leipnik system via fractional caputo-fabrizio derivatives. *Sci. Rep.*, 13:22726, 2023.

[44] N. Almutairi and S. Saber. Chaos control and numerical solution of time-varying fractional newton-leipnik system using fractional atangana-baleanu derivatives. *AIMS Mathematics*, 8(11):25863–25887, 2023.

[45] N. Almutairi and S. Saber. Application of a time-fractal fractional derivative with a power-law kernel to the burke-shaw system based on newton's interpolation polynomials. *MethodsX*, 12:102510, December 2023.

[46] Khalid I.A. Ahmed, Haroon D.S. Adam, Najat Almutairi, and Sayed Saber. Analytical solutions for a class of variable-order fractional liu system under time-dependent variable coefficients. *Results Phys.*, 56:107311, 2024.

[47] R. L. Bagley and R. A. Calico. Fractional order state equations for the control of

viscoelastically damped structures. *J. Guid. Control Dyn.*, 14:304–311, 1991.
[48] O. Heaviside. *Electromagnetic Theory.* Chelsea, New York, 1971.
[49] D. Kusnezov, A. Bulgac, and G. D. Dang. Quantum levy processes and fractional kinetics. *Phys. Rev. Lett.*, 82:1136, 1999.
[50] H. A. Hammad, M. Qasymeh, and M. Abdel-Aty. Existence and stability results for a langevin system with caputo–hadamard fractional operators. *Int. J. Geom. Methods Mod. Phys.*, 21:2450218, 2024.
[51] K. Tornheim. Are metabolic oscillations responsible for normal oscillatory insulin secretion? *Diabetes*, 46(9):1375–1380, 1997.
[52] S. Saber et al. A mathematical model of glucose-insulin interaction with time delay. *J Appl Computat Math*, 7(3), 2018.
[53] M. H. Alshehri et al. A caputo (discretization) fractional-order model of glucose-insulin interaction: Numerical solution and comparisons with experimental data. *J. Taibah Univ. Sci.*, 15:26–36, 2021.
[54] S. Saber and A. Alalyani. Stability analysis and numerical simulations of ivgtt glucose-insulin interaction models with two time delays. *Math. Model. Anal.*, 27:383–407, 2022.
[55] M. H. Alshehri, S. Saber, and F. Z. Duraihem. Dynamical analysis of fractional-order of ivgtt glucose–insulin interaction. *Int. J. Nonlin. Sci. Num.*, 24:1123–1140, 2023.
[56] K. I. A. Ahmed et al. A comprehensive investigation of fractional glucose-insulin dynamics: existence, stability, and numerical comparisons using residual power series and generalized runge-kutta methods. *Journal of Taibah University for Science*, 19(1), 2025.
[57] A. Atangana. Fractal-fractional differentiation and integration: Connecting fractal calculus and fractional calculus to predict complex systems. *Chaos Solitons Fractals*, 102:396–406, 2017.
[58] K. I. A. Ahmed, H. D. S. Adam, and S. Saber. Different strategies for diabetes by mathematical modeling: Applications of fractal-fractional derivatives in the sense of atangana-baleanu. *Results in Physics*, 26:106892, 2023.
[59] K. I. A. Ahmed et al. Different strategies for diabetes by mathematical modeling: Modified minimal model. *Alexandria Engineering Journal*, 80:74–87, 2023.
[60] H. Khan, J. Alzabut, A. Shah, et al. A study on the fractal-fractional tobacco smoking model. *AIMS Math.*, 7:13887–13909, 2022.
[61] H. Khan, A.H. Rajpar, J. Alzabut, et al. On a fractal–fractional-based modeling for influenza and its analytical results. *Qual. Theory Dyn. Syst.*, 23:70, 2024.
[62] Kamaledin Abodayeh, Ali Raza, Muhammad Rafiq, et al. Analysis of pneumonia model via efficient computing techniques. *Computers, Materials & Continua*, 70(3):6073–6088, 2022.
[63] S.M. Ulam. *A Collection of Mathematical Problems.* Interscience Publ., New York, 1960.
[64] Stanislaw M Ulam. *Problems in modern mathematics.* Courier Corporation, 2004.